Thermochemical sorption heat storage: Investigate the heat released from activated carbon beads used as porous host matrix for MgSO4 salt

Minh Hoang Nguyen, Mohamed Zbair, Patrick Dutournié, Simona Bennici

Thermochemical sorption heat storage: Investigate the heat released from activated carbon beads used as porous host matrix for $MgSO_4$ salt

Minh Hoang Nguyen[1,2], Mohamed Zbair[1,2], Patrick Dutournié[1,2], and Simona Bennici [1,2]*

[1] Institut de Science des Matériaux de Mulhouse (IS2M), Université de Haute-Alsace, CNRS, IS2M UMR 7361,
F-68100 Mulhouse, France; minh-hoang.nguyen@uha.fr; mohamed.zbair@uha.fr; patrick.dutournié@uha.fr; cyril.vaulot@uha.fr; ludovic.josien@uha.fr; simona.bennici@uha.fr

[2] Université de Strasbourg, France

* Correspondance: simona.bennici@uha.fr; Tel.: +33 (0)3 89336729

Highlights

- $MgSO_4$/bead activated carbon composites materials were synthesised using impregnation method.
- The composites present relatively high heat storage capacities.
- The composites showed an enhanced mass transfer.
- Composite salt of 7.5 wt% of salt has a good stability over 10 hydration/dehydration cycles.

Abstract:

$MgSO_4$/bead activated carbon composites have been investigated in thermochemical sorption heat storage. The bead activated carbon (BAC) has a high degree of micro-porosity and a large surface area of about 1300 m^2/g, making it a potential candidate as support for salt/support composites for thermochemical heat storage. Furthermore, the thermal conductivity of BAC was measured and a value of 0.14 W/mK was recorded (which is higher than that measured for other supports such as zeolites or alumina). After deposition of $MgSO_4$ by wet-impregnation, the specific surface area

decreased, but the pore size distribution of the carbon matrix was preserved. The water sorption capacity of BAC was 0.138 g/g in stationary conditions (RH=60%, gas flow= 40ml/min). This value was 2.32 times higher for the composite 7.6-$MgSO_4$/BAC due to the dispersion of the salt in the host matrix. An adsorption capacity higher than the calculated value was observed, which could be due to the condensation of water molecules within the porous structure, and thus a higher thermal energy density than calculated one was recorded. The 7.6-$MgSO_4$/BAC composite achieved the highest heat of hydration of 838 J/g. 10 cycles (dehydration at 150 °C and hydration at 30 °C with a relative humidity of 60%) were performed and confirmed the composite's excellent stability.

Keywords: Thermochemical heat storage; magnesium sulfate; bead activated carbon; water sorption; adsorption kinetics.

1. Introduction

Energy supply, as a global important concern, is raising more awareness than ever, especially with the exponential expansion of the population. Fossil fuels have provided nearly 80% of global energy since the mid-twentieth century [1], and the reserves are being exploited indiscriminately [2]. Transitioning to solar energy systems as an alternative source of energy is advocated as a way to reduce greenhouse gas emissions from fossil fuel consumption [3,4].

A large contribution of solar energy can be harvested and used in the built environment as this sector is responsible for over one third of the world energy consumption [5,6]. This natural source of energy is however weather dependent; energy is delivered during shining hours and none is created during off-sun hours. Thermal energy storage (TES) is an advanced technology and an effective solution to resolve the mismatch between supply and demand, as well as long-term solar energy use [7–9]. Latent heat storage, sensible heat storage, and thermochemical heat storage

(TCHS) are three types of system using TES technologies. While sensible heat storage is widely commercially known and latent heat storage are extensively studied [10,11], there have been less attention on TCHS, which is becoming a focal point in the domain due to its higher energy storage density and theoretically no heat loss over time [12–14]. The principle is based on the reversible sorption reaction where heat is stored during desorption (charge) and then released when needed during adsorption (discharge). To turn the system into a practical residential application (space heating and sanitary hot water), the TCHS material needs to be chosen with care. Certain properties such as high energy density, low charging temperature with a good mass and heat transfer [15,16], improved thermal conductivity [17] are used as criteria for choosing salt hydrates as the potential candidate [18–20]. Thanks to the high theoretical energy density (2.8 GJ/m^3) and high deliquescence relative humidity (DRH) of 90 %, the couple $MgSO_4$-H_2O has been attracting growing interests [21,22]. Though, the performance did not meet expectations due to the kinetic hindrance and formation of aggregates. Dispersing the salt inside a porous host matrix is the proposed solution in order to achieve the full potential energy of $MgSO_4$. Wang et al. [23] impregnated 15%wt. $MgSO_4$ onto a zeolite 13X and the heat released reached 632 $J/g_{composite}$ after hydration at 25°C using 80 % RH. Another interesting choice of porous support is activated carbon (AC). ACs present extremely high specific surface area that facilitates the water vapor sorption rate and provides higher heat storage capacity (for hydration cycles of fixed time). Akcaoglu et al. [24] measured the hydration heat released by pellets composites of $MgSO_4$/AC. A very high value of heat storage density (1395 $J/g_{composite}$) was found. For this reason and for practical application the beads activated carbon (BAC) has been selected as a porous support for the impregnation of $MgSO_4$ in this paper. Our main objective is to gain insight on the impact of $MgSO_4$ salt on the hydration behaviors when it is confined inside beads activated carbon pores.

2. Materials and Methods

2.1. Preparation of composites $MgSO_4$/BAC

Composite materials made of $MgSO_4$ and BAC (99.8%, Kureha Corp.) (average particle radius of BAC is R_p = 0.35 mm) at different compositions were prepared using the Wet Impregnation method. Prior to impregnation, 3 g of BAC were dried in the oven at 150 °C to vaporize any traces of water residue. Then, 10 mL of an aqueous solution of $MgSO_4.7H_2O$ (99.9%, Sigma-Aldrich) at 3 different concentrations were added into the BAC. The mixture solid-liquid were mixed for 24 h so that the salt can be slowly deposited inside the BAC structure before being filtered through the Büchner funnel. The impregnated materials were finally oven-dried at 150 °C for 12 h. Figure 1 summarizes schematically the preparation. Accordingly, three composites were prepared and then labelled as x-$MgSO_4$/BAC (1st column in Table 1) with x is the content of $MgSO_4$ in the composites, determined by X-ray Fluorescence.

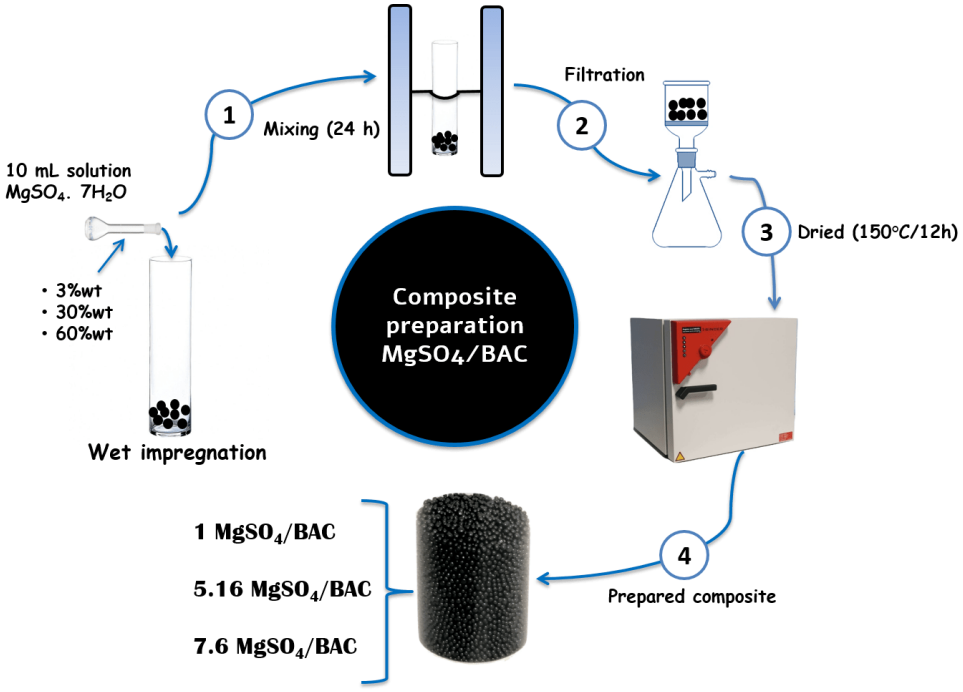

Figure 1. Preparation of composite materials $MgSO_4$/BAC.

2.2. Physicochemical characterizations methods

X-Ray Diffraction (XRD) analyses were performed on the powder of the samples (beads were ground into fine particles) on a diffractometer PANalytical MPD X'Pert

Pro, equipped with a Pixcel real-time multiple strip detector, operating with an angular aperture of 3.347° 2θ in 3° to 80° 2θ range, and using CuKα radiation with 0.15418 nm wavelength. Diffractograms were recorded at 22 °C with a step size of 0.013° 2θ and a scan time of 220 s per step.

A wavelength dispersion X-Ray Fluorescence (WDXRF) spectrometer (from PANalytical, Zetium) was used to perform the XRF measurements on pellets made of 0.1 g of the sample and 0.2 g of binder boric acid (H_3BO_3).

High-resolution micrographics were acquired by a Scanning Electron Microscope (SEM) from JEOL, JSM-7900F model. The semi-quantitative chemical analysis and atomic composition mapping of the sample was performed by means of Energy Dispersive X-ray (EDX).

N_2 adsorption/desorption isotherms of support and composites at -196 °C were acquired in a ASAP 2420 device from Micrometrics. The samples were previously degassed at 150°C for 12 h and then, again at 150 °C for 2 h directly on the analysis port before analysis. The specific surface area was calculated applying the Brunauer, Emmett and Teller (BET) equation (S_{BET}). The micoporous volumes (Vm) and surfaces (Sm) were determined by applying the Dubinin-Astakhov's model. In this model, the exponent N was checked to be very closed to 2. The external surface (S_{ext}) was considered as the non-microporous surface which was calculated by the t-plot method. The mesoporous volume (V_{meso}) compare the total pore volume Vp with the Vm. Finally, the pore size distribution (PSD) was determined using Density Functional Theory (DFT) calculations. A geometry in slit and a carbon surface provided the best fitting and the most logical model for the DFT calculation. CO_2 adsorption/desorption isotherms at 0 °C were also performed with the same equipment to observe more efficiently the ultra-microporosity, which was not accessible to the N_2 molecules. The slit geometry and the CO_2-DFT model were also applied to this last experiment.

The apparent thermal conductivity of the porous support (BAC) was measured according to a transcient method (hot-wire method, using a TLS-100 apparatus from

Thermtest Inc., Fredericton, Canada). The material was placed in a cylindric box (ϕ = 50 mm, L = 120 mm) and the probe (100 mm length) was centered in the middle of the cylinder.

The heat capacity ($\rho\ C_p$) of the material was measured by using a Hot Disk thermal analyser with a Kapton 8563 F1 sensor from Hot Disk AB, Gothenburg, Sweden. The material was placed in a cuboid box (L = 70, l = 70 and h = 60mm). The probe sensor was placed in the middle of the box (at h = 30 mm), so that the heat transfers are simmetric.

2.3. Hydration experiments

The heat released and water adsorption quantities (measured by the microbalance) of the BAC and its composites were measured using a Sensys TG-DSC (thermogravimetry coupled to differential scanning calorimetry) device and a Wetsys flow humidity generator, both from Setaram. The samples (10 mg) were dehydrated at 150 °C before hydration by increasing the temperature from 30 to 150 °C at 5 °C/min under a flow of dry air (30 mL/min), followed by a 3 h isotherm at 150 °C for complete dehydration. The relative humidity (RH) was increased to 60% (a pressure of 2.55 kPa) once the temperature was reduced to 30 °C and the DSC signal attained a stable baseline. To completely rehydrate the material, the hydration procedure was set for 8 hours; total rehydration was attained when the DSC signal returned to the baseline. The samples' hydration heat (J/g_{sample}) was deduced from the surface's intergration beneath the DSC signal during hydration. These conditions are quite similar to those that would be found in a building: 150 °C is a temperature that may be easily obtained with flat-plate solar heat collectors [25,26], while 30 °C is close to the temperature of the inside air during the discharging phase [27].

3. Results and discussion

3.1. Thermal and Structural properties of the composite materials

The apparent thermal conductivity of the porous support at room temperature (hydric and thermal balance) was measured by using a hot wire probe. At 20 °C the apparent thermal conductivity was λ = 0.14 $Wm^{-1}K^{-1}$ with a maximal relative error of 3.4% (8 tests).

The thermal conductivity and the heat capacity were also investigated by using a hot disk apparatus. A previous study [28] showed that measurements of heat capacity, thermal diffusivity, and thermal conductivity were not satisfactory. Indeed, this technique actually measured the thermal effusivity of the material. The thermal effusivity is E = 316 $JK^{-1}m^{-2}$ $s^{-0.5}$ with a maximal relative error inferior to 10% (12 experiments). Starting from these previous results (E and λ), the heat capacity could be calculated ($\rho\, C_p = \frac{E^2}{\lambda}$ = 0.71 $MJm^{-3}K^{-1}$) and assuming an apparent density (600 kgm^{-3}, manufacturer data), the specific heat capacity was determined: C_p= 1190 $Jkg^{-1}K^{-1}$.

The addition of hydrated salt should improve the thermal properties of the material since the thermal conductivity and the specific heat capacity of hepta-hydrated salt are 0.45 $Wm^{-1}K^{-1}$ and 1600 $Jkg^{-1}K^{-1}$, respectively.

The thermal properties of these composite materials are better than those of classical adsorptive materials. For example, the thermophysical properties of dry zeolite 13X at 298K (widely used for thermochemical heat storage applications) are 0.075 $Wm^{-1}K^{-1}$ and 900 $Jkg^{-1}K^{-1}$ for thermal conductivity and specific heat capacity, respectively.

Table 1 summarizes the chemical composition acquired using the WDXRF method as well as the textural characteristics (S_{BET}, S_{ext}, S_m, V_p, V_m, and V_{meso}). Different concentrations of solution $MgSO_4.7H_2O$ have led to different amounts of $MgSO_4$ anhydrous deposited in the BAC structure. As the $MgSO_4$ loading increases, the S_{BET} and V_p values of the BAC and related composites show a slight decrease. The size of some pore entrances can be hindered by the presence of $MgSO_4$ particles after impregnation, resulting in the pore inaccessibility by N_2 molecules. This explains why the S_{BET} of the BAC (1295 $m^2.\ g^{-1}$) was reduced by 13.6 % when 7.6 %of $MgSO_4$ was

added. In addition, as compared to pure BAC, the V_p of the composite 7.6-$MgSO_4$/BAC (0.48 $cm^3.g^{-1}$) was decreased just by 12.7%. $MgSO_4$ deposition, on the other hand, has no effect on the form of the supports' N_2-adsorption isotherms (**Figure 2a**).

BAC support and prepared composites display type Ib isotherm (**Figure 2a**) according to Rouquerol et al. [29]. A vertical adsorption line at very low relative pressure (0.01 p/p°) is followed by a convex curve and a plateau towards p/p° = 1. Microporous (pore size < 2 nm) materials are indicated by high adsorption at very low p/p°. The micropores are narrower when the line is sharper. The PSD of the composites and pure BAC shown in **Figure 2b** has been obtained by applying the DFT method with the NLDFT model.

All the samples, including the BAC and the composites, show the same distribution of pores (only the V_p decreases) with three peaks located at 0.8, 1.2, and 1.7 nm. This distribution validates that the BAC and its composites are highly microporous materials. This was also demonstrated by the microporous surface (S_m) ratio, which accounts for approximately 85% of the S_{BET} after impregnation. With the maintenance of the PSD of the composites, the pore sizes are clearly not affected. Thus, the decrease of V_p is due to the fact that certain pores were completely blocked by aggregates of salt particles.

To fully grasp the information on the microporous structure, CO_2 adsorption (0 °C) was performed (**Figure 2c**) on all samples to investigate the ultra-micropores (< 1 nm).

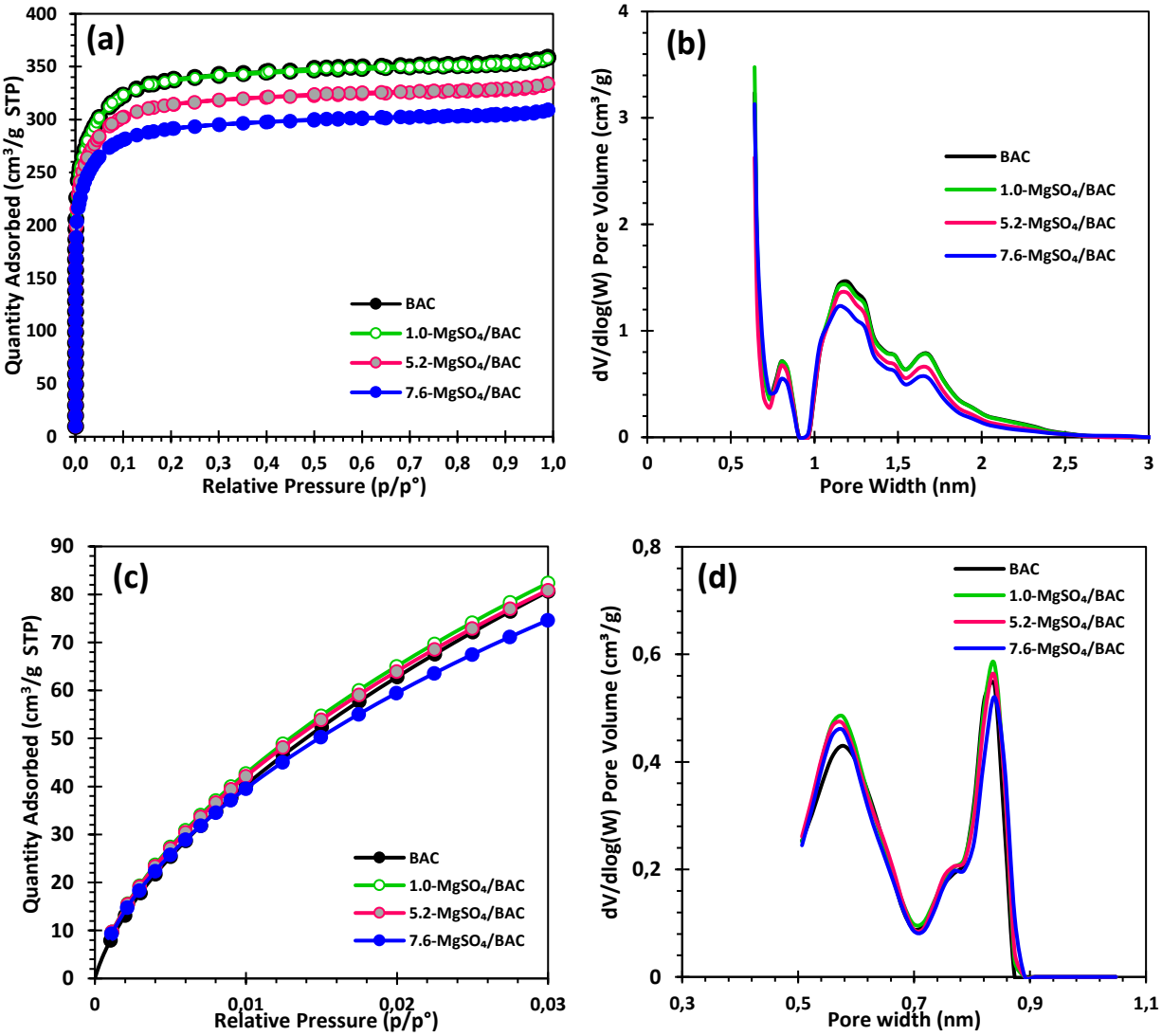

Figure 2. (a) N_2 adsorption-desorption isotherms, **(b)** PSD (N_2) of BAC and its composites with $MgSO_4$, **(c)** CO_2 adsorption isotherms, **(d)** PSD (CO_2) of BAC and its composites with $MgSO_4$.

Figure 2d shows the PSD of these samples using the CO_2-DFT calculations with two main peaks located at 0.58 nm and 0.84 nm. With the presence of the $MgSO_4$ particles the specific surface as well as the porous volume of the impregnated samples decreased slightly compared to the BAC (**see Table 2**). Furthermore, the PSD CO_2 adsorption are the same for all samples (**Figure 2d**) which led to a conclusion that there is no influence on the pore sizes. As the porous volume decreases slightly, there are certain pores were also completely blocked by the salt aggregates, thus reduces the

dispersion of the salt as well as the $MgSO_4/H_2O$ interaction surfaces. As a result, the overall performance of these materials can be significantly impacted in terms of thermal energy released.

Table 1. Physicochemical characteristics of BAC support and $MgSO_4$/BAC composites obtained from N_2 (-196 °C) adsorption isotherm data.

Sample	$MgSO_4$ content (wt%)	S_{BET} ($m^2.g^{-1}$) [a]	S_m ($m^2.g^{-1}$) [b]	S_{ext} ($m^2.g^{-1}$) [b]	V_p ($cm^3.g^{-1}$) [c]	V_m ($cm^3.g^{-1}$) [b]	V_{meso} ($cm^3.g^{-1}$) [b]
BAC	-	1295	1096	199	0.55	0.438	0.112
1.0-$MgSO_4$/BAC	1.0	1293	1099	194	0.55	0.439	0.111
5.2-$MgSO_4$/BAC	5.2	1210	1036	174	0.52	0.413	0.107
7.6-$MgSO_4$/BAC	7.6	1123	991	132	0.48	0.396	0.084

[a] Calculated using the BET equation in the range 0.01-0.1 p/p° (cross-sectional area of 0.162 nm^2).

[b] Determined using the Dubinin-Astakhov equation in the range 10^{-4} – 0.01 p/p°.

[c] Determined from the amount of N_2 adsorbed at p/p°=0.99.

Table 2. Physicochemical characteristics of BAC support and $MgSO_4$/BAC composites obtained from CO_2 (0 °C) adsorption isotherm data.

Sample	$MgSO_4$ content (wt%)	S_{BET} ($m^2.g^{-1}$) [a]	V_p ($cm^3.g^{-1}$) [b]
BAC	-	653	0.1498
1.0-$MgSO_4$/BAC	1.0	646	0.1498
5.2-$MgSO_4$/BAC	5.2	619	0.1468
7.6-$MgSO_4$/BAC	7.6	562	0.1358

[a]Calculated using the BET equation in the range 0.009-0.03 p/p° (cross-sectional area of 0.170 nm^2).

[b] Determined from the amount of CO_2 adsorbed at p/p°=0.03.

To further investigate the surface structure and the morphology, a series of characterizations (SEM, EDX and XRD) were conducted on the three composites and on the commercial BAC.

SEM and EDX mapping of pure BAC support and BAC-based composites were used to gain insight about the morphology and homogeneity of the $MgSO_4$ deposition on the surface (**Figure 3**). In all samples, a smooth surface with a high carbon content is detected. The composites presented a homogeneous surface with no macro $MgSO_4$ crystallites. EDX mapping study also confirmed the uniformity of the $MgSO_4$ deposition on all composites. This finding is corroborated by the XRD diffractograms that do not show any peak corresponding to $MgSO_4$: large crystallites were absent in all the BAC-based composites.

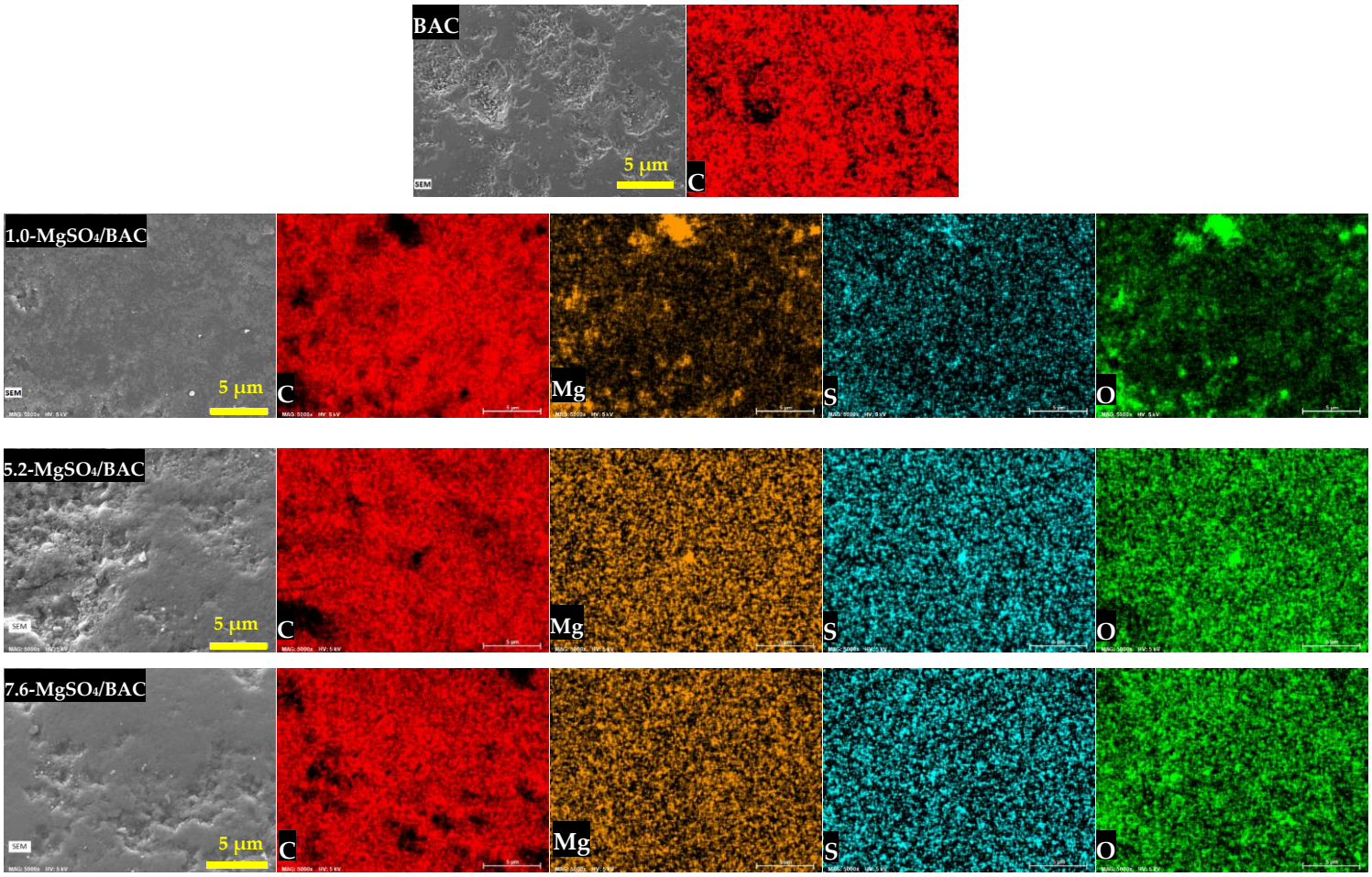

Figure 3. SEM images of BAC original and its composites with $MgSO_4$.

The XRD patterns of pristine BAC and related composites (**Figure 4**) presented two broad diffraction peaks at 24° and 43°, corresponding to two planes (002) and (100) which are reflections of graphitic plane and disordered graphitic plane, respectively [30,31]. There were no reflections detected associated to $MgSO_4$ in the BAC-$MgSO_4$ series of composites. This is an indication of the presence of an amorphous phase of partially hydrated $MgSO_4$ [21,26] formed during the deposition step or to the presence of very small salt crystallites with dimension below the XRD spectrometer detection level. This latter leads to the absence of well-defined peaks related to $MgSO_4$ on the XRD patterns.

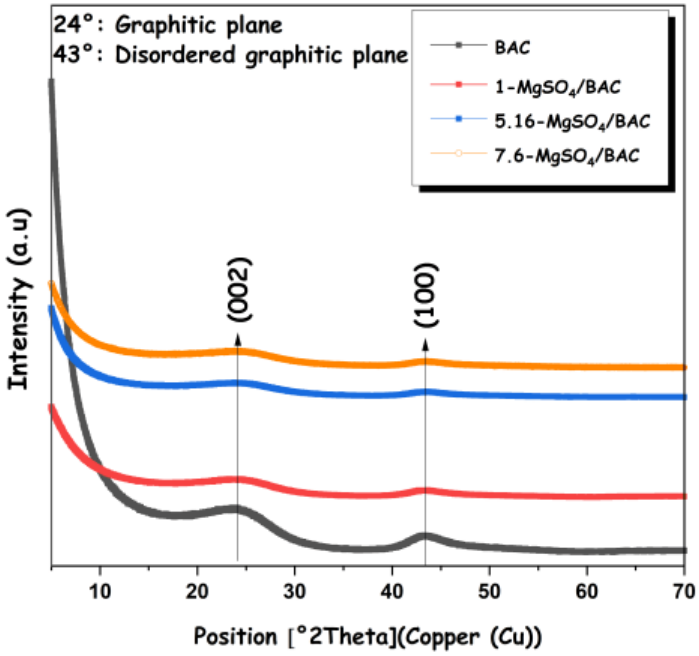

Figure 4. XRD patterns of BAC and its composites.

3.2. TG-DSC analysis for hydration behaviors

A TG-DSC device was used to measure the hydration heat released and water sorption capacities of the BAC support and its composites under controlled temperature and pressure. The mechanism of the hydration process is illustrated as in **Figure 5**.

The heat produced upon hydration (**Figure 5a**) and the water adsorption capacity (designated as "w_e" in Equation (1)) (**Figure 5b**) were calculated from the variation of

the heat flow and the mass of the sample as a function of time. The water adsorption mechanism on the composite storage material is also illustrated in **Figure 5c**. Heat production and water uptake in three manufactured composites rose as salt concentration increased. Indeed, when more salt was deposited onto the porous structure, the contact surface between salt particles and water vapor expands greatly. Therefore, more exothermic reactions took place leading to a more sizeable thermal energy density.

$$w_e = \frac{m_h - m_d}{m_d} \qquad (1)$$

where w_e is the water adsorption capacity (gH_2O/g_{sample} or g/g in short), m_h (g) and m_d (g) correspond respectively to the final mass of the hydrated sample and the dehydrated sample. However, these values doubled their respective calculated ones which are shown in **Table 3**.

The calculated values are made from the contribution of the $MgSO_4$ salt and of the porous BAC support based on their respective content in the composites. Although the BAC support (BAC/H_2O interaction) contributed a certain amount to the overall heat storage density, it did not have a significant impact.

The contribution from the exothermic reaction $MgSO_4/H_2O$ is the most important since it is the main energy source of the system. There was another source of thermal energy which comes from the condensation of water molecules on another layer of water molecules (first layer in contact with $MgSO_4$ particles) or from the formation of a saturated solution of $MgSO_4$ resulting from overhydration [32].

The overhydration in general takes place whenever the RH during the adsorption is greater than the DRH of the salt. In this paper, the operating conditions are 30 °C and 60 %RH while the DRH of $MgSO_4$ is about 90 %; so the chance of forming a saturated solution is minimal. Accordingly, the energies obtained experimentally that are higher than the calculated ones are dued to the condensation of water molecules in the pores strucuter of BAC. **Table 4** compares the performance of the 7.6-$MgSO_4$/BAC composite

to other composites storage material reported in the litteratures which show a better performance of this composite over certains reported materials.

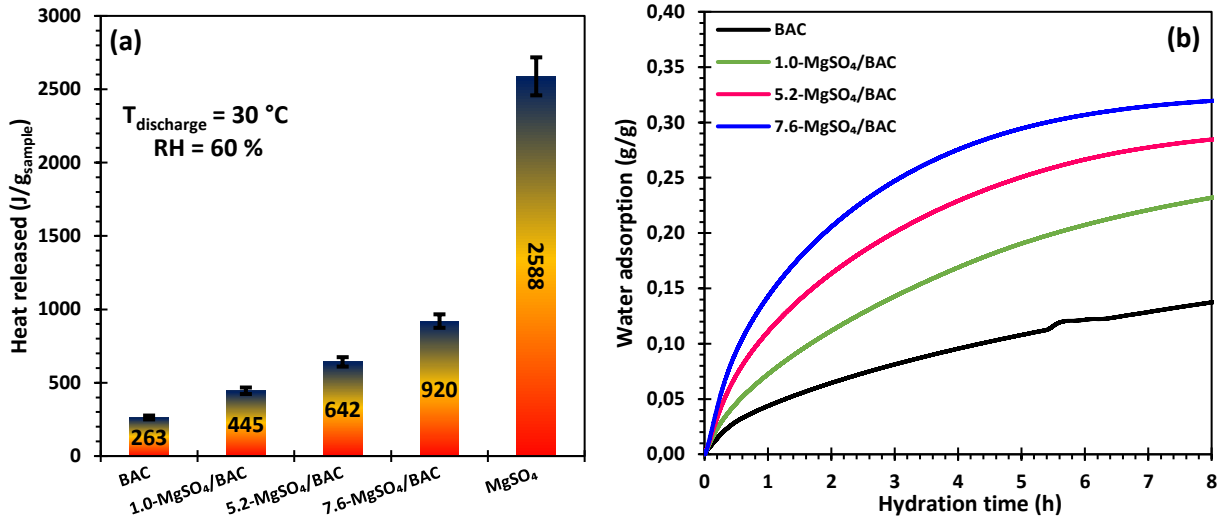

Figure 5. (a) Hydration behavior of $MgSO_4$ and BAC composites at 30 °C and 60 %RH **(b)** Water adsorption curves of BAC support and composites ($T_{discharge}$ = 30 °C; RH = 60 %; 8 h of hydration)

BAC seul, les mesures de heat released and water adsorption montrent que heat released per gram of water is close to the latent heat of water (Lv ≈ 2300 J/g_{water})

The theoretical heat released of impragnated materials are estimated by adding heat of salt hydration (from 1 to 6 water molecules), i.e. ΔH_{exp} = 3200 J/g_{water} and latent heat of water according to the equation XX

$$Q = S\% * (6-1) * \frac{18}{120.4} * \Delta H_{exp} + Lv * \left(W_{exp} - S\% * (6-1) * \frac{18}{120.4}\right)$$

Table 3. Experimental results and calculated values of $MgSO_4$, BAC and its composites.

Sample	Heat released Q_{exp} (J/g_{sample})	Heat released calculated Q (J/g_{sample})[b]	Water adsorption W_{exp} (g/g)	Water adsorption calculated (g/g)[b]
$MgSO_4$ [a]	2588	-	0.809	-
BAC	263	-	0.138	-

1.0-$MgSO_4$/BAC	445	540	0.232	0.151
5.2-$MgSO_4$/BAC	642	688	0.284	0.179
7.6-$MgSO_4$/BAC	920	902	0.370	0.194

[a] Determined experimentally by TG-DSC/Wetsys.

[b] Calculated by addition of the heat contribution of $MgSO_4$ salt and BAC support in each sample.

Table 4. Comparaison of 7.6-MgSO4/BAC with other sulfate-based composited in the litteratures.

Composite materials	Operating conditions	Energy storage density (J/g)	Reference	Year
7.6-$MgSO_4$/BAC	**T_{hyd} = 30 °C; RH = 60%**	**920**	**This work**	**2022**
20-$MgSO_4$/HAP	T_{hyd} = 30 °C; RH = 60%	464	[33]	2022
30-$MgSO_4$/Diatomite (D30)	T_{hyd} = 25 °C; RH = 80%	460	[34]	2021
60-$MgSO_4$/Diatomite (D60)		773		
50-$MgSO_4$/Expanded graphite (EG50)	T_{hyd} = 25 °C; RH = 85%	496.4	[35]	2021
$MgSO_4$/13x with %$MgSO_4$ up to 20%	T_{hyd} = 25 °C; RH = 60%	510–575	[23]	2019
$MgSO_4$/zeolite (laboratory pilot)	T_{hyd} = 25 °C; RH = 85%	401	[8]	2018
$MgSO_4$/zeolite Modernite	T_{hyd} = 22 °C; RH = 50%	507	[26]	2013
$MgSO_4$/zeolites H-Y		867	[36]	2013

$MgSO_4$/zeolites Na-Y	T_{hyd} = 20 °C; RH = 55%	1090	

3.3. Hydration kinetic modeling

According to **Figure 5b**, BAC supports and composites adsorb water at different rates. Visually, water sorption occurs quickly at the beginning for all samples, then becomes sluggish over the hydration time. It is observed that after the first hour, the BAC adsorption capacity is already at two-thirds of the equilibrium level, while the impregnated composites adsorb around half of the maximum capacity. After that, the kinetics of all samples decreased substantially. While the kinetic curve of the BAC support reached equilibrium after 6 h of hydration, the prepared composites approached their respective equilibriums at the 7th hour of hydration. The amount of salt deposited appears to have the highest impact on the hydration behavior. As the salt concentration increases, the water vapor diffusion becomes less favorable and, thus, more time is required for the hydration reaction to take place.

In order to investigate the kinetics of water adsorption onto BAC composites more deeply, different kinetic models: pseudo first order, intraparticular diffusion, diffusion into homogeneous material (Crank's diffusion model), diffusion through a surended salt layer and Elovich) have been applied (**Table 5**). The fitting results are then reported in **Figure 6**, and the obtained kinetic parameters are listed in **Table 6.**

Table 5: Non-linear kinetic adsorption models.

Kinetic model	Equation	Description of parameters	Ref.
Pseudo First Order (PFO)	$w_t = w_e[1 - \exp(-K_1 t)]$	w_t is the water uptake at time t ($g_{water}/g_{composite}$), w_e: the water uptake at equilibrium ($g_{water}/g_{composite}$), t is the hydration time (h), K_1 is the rate constant of	[37–39]
Intraparticule diffusion (IPD)	$w_t = k_{Id}\sqrt{t} + C$		

		the PFO model (s^{-1}) and k_{id} is the rate constant of the IPD model ($g_{composite}/g_{water}.s^{-0.5}$)	
Crank's diffusion	$w_t = w_e(1 - \sum_{n=1} \frac{6}{n^2\pi^2} e^{-\frac{n^2\pi^2 Dt}{R^2}})$	D_t is the apparent diffusion coefficient (m^2/s), R the particle radius	[doi:10.1016/j.cej.2009.04.042 | Elsevier Enhanced Reader
Layer diffusion	$w_t = w_e(1 - \sum_{k=0} \frac{8}{(2k+1)^2\pi^2} e^{-\frac{(2k+1)^2\pi^2 Dt}{e^2}})$	e is the layer thichness (m) calculated according to salt mass balance	
Elovich	$w_t = E_0 + E_1 \ln(t)$	E_0, E_1 are Elovich equation parameters	[39,40]

The PFO model are often used in the literature for studying the adsorption kinetic of water in heat storage materials. This model used for liquid phase, assumes a sorption kinetic proportional to the difference of concentration at the surface. The limiting step of this model is the physisorption. The intraparticle diffusion modelling assumed that the diffusion is the right limiting step of water sorption in the particle. The Crank's model assumes that the water diffuses in a homogeneous and porous spherical particles. The fourth assumes that the impragnated salt forms a layer around the BAC. The thichness of this layer is calculated respecting salt mass balance, and the mass transfer in this layer is assumed to be diffusive. The last one (Elovich model) is a logarithmic rate law for describing chimisorption in porous solids. His use don't considerate mechanisms limited by gazeous diffusion, as for example Kundsen diffusion.

The first observation is that the PFO and the Elovich models don't discrible accurately the experimental kinetics, especially the beginning of hydration. The form of these two equations doesn't allow fitting well the experimental data. In the same way, the two

diffusive models (crank and salt layer) are not a good numerical approximation of the experimental results. First, the model coming from differential equation of diffusive mass transfer doesn't describe diffusive mechanisms in a microporous material. For the diffusive model through a salt layer, the uncertainty of the layer thickness estimation (calculated by respecting salt mass balance) is the major issue for obtaining good numerical approximation.

Unlike the other ones, the intraparticle model proposed by Weber and Morris allows fitting well the experimental data as shown in figure X. It has been widely applied for the study of adsorption kinetics in different porous materials (micro, meso and macro). The slope of the linear curve increases with the amount of impragnated salt and this rate kinetic constant is quasi independent of the salt concentration when it is divided by the water uptake at equilibrium. This indicates that the mechanisms of adsorption are the same and with the same intensities irrespective of the amount of impragnated salt.

Figure 6. Application of three different kinetics model (PFO, PSO and Elovich) on the adsorption kinetics of BAC and composites at different salt contents.

Table 6. The kinetic parameters obtained from different adsorption kinetic models.

	BAC	1.0-$MgSO_4$/BAC	5.2-$MgSO_4$/BAC	7.6-$MgSO_4$/BAC
Pseudo First Order (PFO)				
$We_{(experimental)}$ (g/g)	**0.138**	**0.232**	**0.285**	**0.319**
$We_{(calcultaed)}$ (g/g)	0.149	0.252	0.289	0.318
K_1 (s^{-1})	0.275	0.289	0.418	0.531
R^2	0.985	0.994	0.992	0.992
Pseudo Second Order (PSO)				
$We_{(calcultaed)}$ (g/g)	0.209	0.353	0.375	0.396
K_2 (s^{-1})	**1.069**	**0.664**	**1.055**	**1.407**
R^2	**0.991**	**0.997**	**0.998**	**0.998**
Elovich				
E_0	0.054	0.093	0.133	0.164
E_1	0.033	0.057	0.070	0.075
R^2	0.885	0.894	0.936	0.955

In **Figure 6**, PFO, PSO, and the Elovich equation were the three kinetic models applied to fit the experimental data corresponding to the amount of adsorbed water vs hydration time. The results of the nonlinear fitting gathered in **Table 6** show the superiority of the PSO model with respect to the other two models. A coefficient of determination R^2 closest to 1 ($R^2 \approx 0.99$) was obtained. However, once the calculated water uptake by the PSO and PFO models is compared to the experimental values, as shown in **Table 6**, the calculated water uptake by the PFO model is extremely close to the experimental values. This suggests that the adsorption process can be well described by the PFO model. It can also be observed that there is a little deviation in the model from the experimental data during the first hour of hydration. The model

suggests a faster hydration at the beginning of the adsorption process then eventually rejoins the experimental curves as the hydration time is extended. Remarkably, the adsorption kinetic rate K_1 of water uptake increased upon increasing the $MgSO_4$ content, confirming that the adsorption process occurred with enhanced mass transfer by increasing the percentage of salt deposited inside the BAC (**Figure 7**).

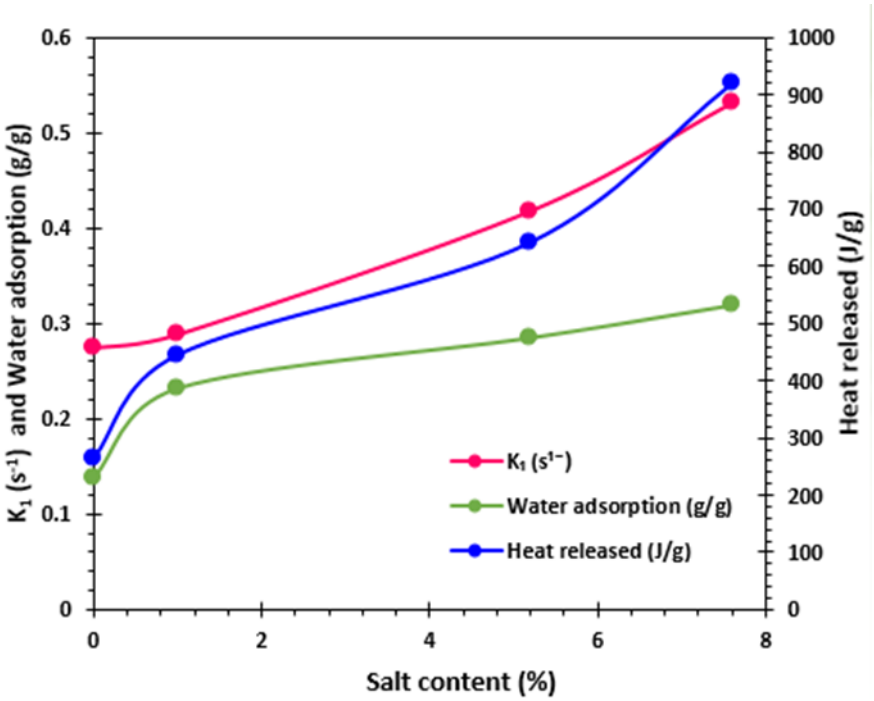

Figure 7: The effecty of salt conent on adsorption kinetic rate, water adsorption and heat released.

3.4. Cyclability and stability of composite 7.6-$MgSO_4$/BAC

As part of the stability testing, the 7.6-$MgSO_4$/BAC composite underwent five consecutive cycles of hydrating and dehydrating at temperatures of 150 °C (dehydration) and 30 °C (hydration) at a RH of 60%. The heat released after each cycle was obtained and compared to the previous ones in order to check if the material was still stable. **Figure 8** shows that just a minor fluctuation (about 10%) in thermal energy density was found among the cycles, confirming the composite's good stability. **Figure 9** shows the EDX images after 1 cycle and after 10 cycles of 7.6-$MgSO_4$/BAC. No

aggregates of salt particles were observed in any images, confirming the cyclability of the prepared composite (7.6-$MgSO_4$/BAC).

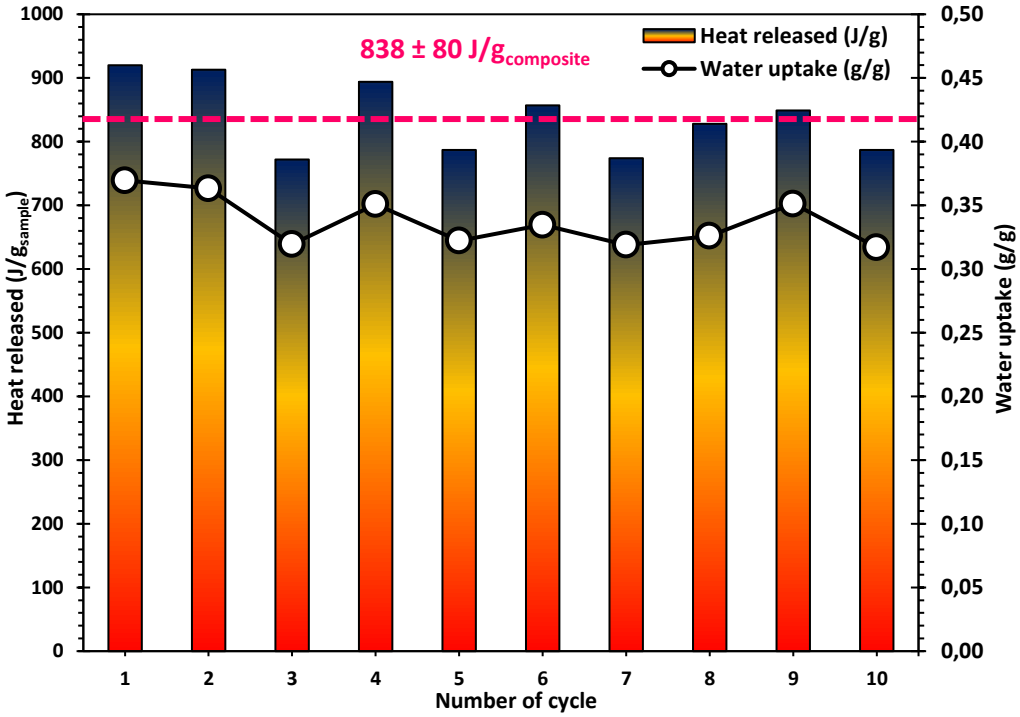

Figure 8. Evaluation of 7.6-$MgSO_4$/BAC composite stability for 10 cycles.

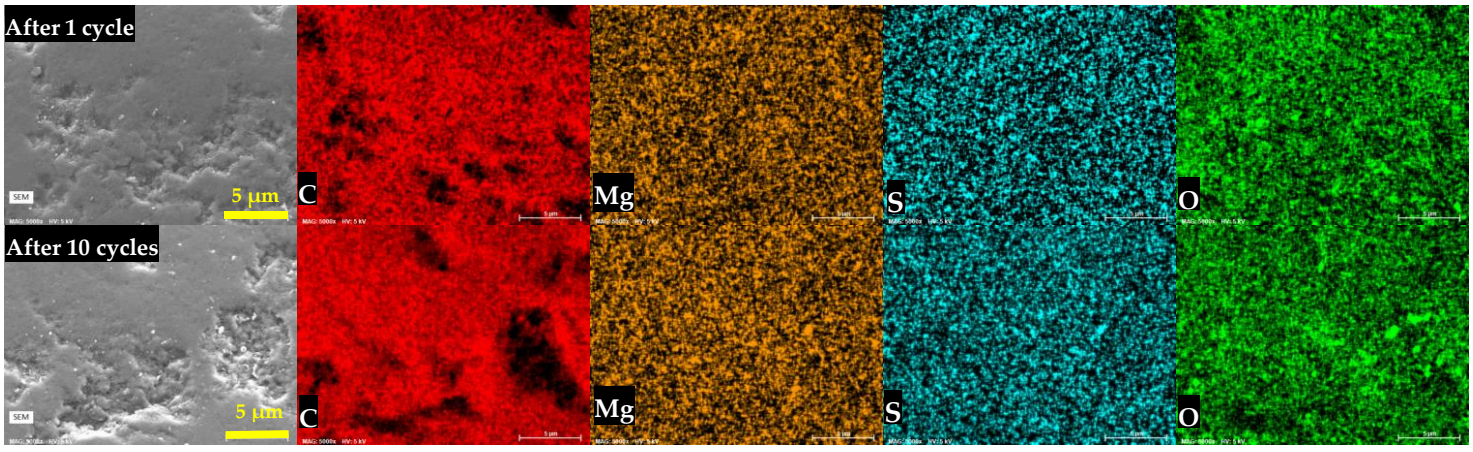

Figure 9. SEM and EDX images of 7.6-$MgSO_4$/BAC after 1 cycles and after 10 cycles.

4. Conclusions

In this work, we investigate the composite of $MgSO_4$ salt impregnated inside beads of activated carbon. It was shown that the composites can be easily prepared by impregnating the salt solutions in the beads with activated carbon. The composites were investigated by a series of physico-chemical methods (XRD, BET, SEM). The 7.6-$MgSO_4$/BAC composite outperforms the other prepared composites with an energy storage density of 920 J/g ($T_{adsorption}$ = 30 °C, $T_{desorption}$ = 150 °C, and RH (%) = 60%). The salt's high dispersion improves composite materials' storage capacity. When choosing a storage material for thermochemical heat storage systems, high heat and water storage capacities aren't the only considerations. The system's utility also necessitates fast water sorption kinetics. The good fitting of the kinetic experimental data with the PSO model equation has been successfully performed, allowing us to determine the rate of controlling adsorption mechanism and diffusion, which are important factors in thermochemical heat storage system design. The repeated stability of $MgSO_4$-BAC is evaluated, revealing that 7.6-$MgSO_4$/BAC composite performance is relatively constant after 10 cycles.

Further study can be focused on the energy storage density improvement, cyclic adsorption and desorption performances, and the corresponding kinetic models of the prepared composites. Besides, it is worthwile to investigate the thermochemical behaviors of the composites inside an experimental-scale reactor.

The BAC composites are very promising heat storage materials, also considering the shape of the final materials that can facilitate the filling of the reactor and improve the fluid-dynamics of the system. The transfer of the water molecules presents in the carrier gas (humid air) is then homogeneous onto the overall material. Due to the use of BAC, hotspots can also be prevented thanks to the relatively high thermal conductivity of the carbon support (when compared to other mineral supports, i.e. zeolithes, alumina, MOFs, silica gels, the aluminophosphate AlPO/SAPO). On one hand, by avoiding the local enhancement of the temperature, the material is preserved by thermal degradation in the long term. On the other hand, by keeping the local

temperature constant, the hydration process is performed under controlled conditions, and the local water adsorption equilibrium is optimized by avoiding desorption phenomena during the hydration step due to the eventual temperature increase.

Author Contributions: Conceptualization and Writing—Original Draft Preparation M. H. N, S.B.; Methodology and Writing—Original Draft Preparation M.Z; Review & Editing-Supervision, S. B., P. D; Nitrogen physisorption analyses, M.H.N, C. V; SEM analyses, L. J; Writing—Review & Editing, Supervision, and Project Administration S. B. All authors have read and agreed to the published version of the manuscript.

Funding: - Region Grand Est for providing funding for the acquisition of the TG-DSC equipment within the "STOCKFATAL" project and for the contribution to Mr. Minh Hoang Nguyen's thesis grant.

- Carnot MICA Institute and Region Grand est for funding part of this study in the frame of the STOCKENER project.

- IS2M for the postdoctoral grant of M. Zbair in the frame of the "Projets Structurants" call.

Institutional Review Board Statement: Not applicable.

Informed Consent Statement: Not applicable.

Data Availability Statement: Not applicable.

Acknowledgments: All physicochemical characterizations were performed on the IS2M technical platforms. The authors are very grateful to L. Michelin (XRF), L. Josien (SEM+EDX), and Cyril Vaulot (N_2 and CO_2 adsorption) experiments for their contribution.

Conflicts of Interest: The authors declare no conflict of interest.

Nomenclature

TES, thermal energy storage;

TCHS, thermochemical heat storage;

BAC, bead activated carbon;

DRH, deliquescence relative humidity;

XRD, X-ray Diffraction;

WDXRF, wavelength-dispersive X-Ray Fluorescence;

SEM, Scanning Electron Microscope;

EDX, Energy Dispersive X-ray;

BET, Brunauer, Emmett and Teller;

PSD, pore size distribution;

DFT, Density Functional Theory;

TG, thermogravimetry;

DSC, Differential Scanning Calorimetry;

RH, relative humidity;

References

[1] Statistical Review of World Energy | Energy economics | Home n.d.

[2] Zou C, Zhao Q, Zhang G, Xiong B. Energy revolution: From a fossil energy era to a new energy era. Nat Gas Ind B 2016;3. https://doi.org/10.1016/j.ngib.2016.02.001.

[3] Vandenbergh MP, Gilligan JM. Beyond politics: The private governance response to climate change. Cambridge University Press; 2017. https://doi.org/10.1017/9781316848555.

[4] Babu KS, Kumar EA. Thermodynamic analysis of compressor operated resorption thermochemical energy storage system for heat storage, combined cooling and heat upgradation. J Energy Storage 2022;50:104659. https://doi.org/10.1016/j.est.2022.104659.

[5] Borri E, Zsembinszki G, Cabeza LF. Recent developments of thermal energy

storage applications in the built environment: A bibliometric analysis and systematic review. Appl Therm Eng 2021;189. https://doi.org/10.1016/j.applthermaleng.2021.116666.

[6] Yang T, Liu W, Kramer GJ, Sun Q. Seasonal thermal energy storage: A techno-economic literature review. Renew Sustain Energy Rev 2021;139. https://doi.org/10.1016/j.rser.2021.110732.

[7] Airò Farulla G, Cellura M, Guarino F, Ferraro M. A Review of Thermochemical Energy Storage Systems for Power Grid Support. Appl Sci 2020;10:3142. https://doi.org/10.3390/app10093142.

[8] Xu C, Yu Z, Xie Y, Ren Y, Ye F, Ju X. Study of the hydration behavior of zeolite-MgSO4 composites for long-term heat storage. Appl Therm Eng 2018;129:250–9. https://doi.org/10.1016/j.applthermaleng.2017.10.031.

[9] Hongois S, Kuznik F, Stevens P, Roux J-J. Development and characterisation of a new MgSO4−zeolite composite for long-term thermal energy storage. Sol Energy Mater Sol Cells 2011;95:1831–7. https://doi.org/10.1016/j.solmat.2011.01.050.

[10] A Comprehensive Review of Thermal Energy Storage. Sustainability 2018;10:191. https://doi.org/10.3390/su10010191.

[11] Li W, Zeng M, Wang Q. Development and performance investigation of MgSO4/SrCl2 composite salt hydrate for mid-low temperature thermochemical heat storage. Sol Energy Mater Sol Cells 2020;210:110509. https://doi.org/10.1016/j.solmat.2020.110509.

[12] N'Tsoukpoe KE, Liu H, Le Pierrès N, Luo L. A review on long-term sorption solar energy storage. Renew Sustain Energy Rev 2009;13:2385–96. https://doi.org/10.1016/j.rser.2009.05.008.

[13] Whiting GT, Grondin D, Stosic D, Bennici S, Auroux A. Zeolite–MgCl2 composites as potential long-term heat storage materials: Influence of zeolite properties on heats of water sorption. Sol Energy Mater Sol Cells 2014;128:289–

95. https://doi.org/10.1016/j.solmat.2014.05.016.

[14] Wu H, Salles F, Zajac J. A Critical Review of Solid Materials for Low-Temperature Thermochemical Storage of Solar Energy Based on Solid-Vapour Adsorption in View of Space Heating Uses. Molecules 2019;24:945. https://doi.org/10.3390/molecules24050945.

[15] Tatsidjodoung P, Le Pierrès N, Luo L. A review of potential materials for thermal energy storage in building applications. Renew Sustain Energy Rev 2013;18:327–49. https://doi.org/10.1016/j.rser.2012.10.025.

[16] Gordeeva LG, Tu YD, Pan Q, Palash ML, Saha BB, Aristov YI, et al. Metal-organic frameworks for energy conversion and water harvesting: A bridge between thermal engineering and material science. Nano Energy 2021;84:105946. https://doi.org/10.1016/j.nanoen.2021.105946.

[17] Bennici S, Dutournié P, Cathalan J, Zbair M, Nguyen MH, Scuiller E, et al. Heat storage: Hydration investigation of MgSO4/active carbon composites, from material development to domestic applications scenarios. Renew Sustain Energy Rev 2022;158:112197. https://doi.org/10.1016/j.rser.2022.112197.

[18] Xu J, Li T, Yan T, Chao J, Wang R. Dehydration kinetics and thermodynamics of magnesium chloride hexahydrate for thermal energy storage. Sol Energy Mater Sol Cells 2021;219:110819. https://doi.org/10.1016/j.solmat.2020.110819.

[19] N'Tsoukpoe KE, Schmidt T, Rammelberg HU, Watts BA, Ruck WKL. A systematic multi-step screening of numerous salt hydrates for low temperature thermochemical energy storage. Appl Energy 2014;124:1–16. https://doi.org/10.1016/j.apenergy.2014.02.053.

[20] Zhao Q, Lin J, Huang H, Xie Z, Xiao Y. Enhancement of heat and mass transfer of potassium carbonate-based thermochemical materials for thermal energy storage. J Energy Storage 2022;50:104259. https://doi.org/10.1016/j.est.2022.104259.

[21] van Essen VM, Zondag HA, Gores JC, Bleijendaal LPJ, Bakker M, Schuitema R,

et al. Characterization of MgSO4 Hydrate for Thermochemical Seasonal Heat Storage. J Sol Energy Eng 2009;131. https://doi.org/10.1115/1.4000275.

[22] Mehrabadi A, Farid M. New salt hydrate composite for low-grade thermal energy storage. Energy 2018;164:194–203. https://doi.org/10.1016/j.energy.2018.08.192.

[23] Wang Q, Xie Y, Ding B, Yu G, Ye F, Xu C. Structure and hydration state characterizations of MgSO4-zeolite 13x composite materials for long-term thermochemical heat storage. Sol Energy Mater Sol Cells 2019;200:110047. https://doi.org/10.1016/j.solmat.2019.110047.

[24] Akcaoglu SC, Sun Z, Moratti SC, Martinopoulos G. Investigation of Novel Composite Materials for Thermochemical Heat Storage Systems. Energies 2020;13:1042. https://doi.org/10.3390/en13051042.

[25] Donkers PAJ, Sögütoglu LC, Huinink HP, Fischer HR, Adan OCG. A review of salt hydrates for seasonal heat storage in domestic applications. Appl Energy 2017;199:45–68. https://doi.org/10.1016/j.apenergy.2017.04.080.

[26] Whiting G, Grondin D, Bennici S, Auroux A. Heats of water sorption studies on zeolite–MgSO4 composites as potential thermochemical heat storage materials. Sol Energy Mater Sol Cells 2013;112:112–9. https://doi.org/10.1016/j.solmat.2013.01.020.

[27] Bennici S, Polimann T, Ondarts M, Gonze E, Vaulot C, Le Pierrès N. Long-term impact of air pollutants on thermochemical heat storage materials. Renew Sustain Energy Rev 2020;117:109473. https://doi.org/10.1016/j.rser.2019.109473.

[28] Elliot S, Patrick D, Mohamed Z, Simona B. Thermo-physical properties measurements of hygroscopic and reactive material (zeolite 13X) for open adsorptive heat storage operation. J Therm Anal Calorim 2022. https://doi.org/10.1007/s10973-022-11439-9.

[29] Rouquerol F, Rouquerol J, Sing K. Assessment of Mesoporosity. Adsorpt. by Powders Porous Solids, Elsevier; 1999, p. 191–217. https://doi.org/10.1016/B978-

012598920-6/50008-7.

[30] Zbair M, Ainassaari K, Drif A, Ojala S, Bottlinger M, Pirilä M, et al. Toward new benchmark adsorbents: preparation and characterization of activated carbon from argan nut shell for bisphenol A removal. Environ Sci Pollut Res 2018. https://doi.org/10.1007/s11356-017-0634-6.

[31] Zbair M, Ainassaari K, El Assal Z, Ojala S, El Ouahedy N, Keiski RL, et al. Steam activation of waste biomass: highly microporous carbon, optimization of bisphenol A, and diuron adsorption by response surface methodology. Environ Sci Pollut Res 2018;25:35657–71. https://doi.org/10.1007/s11356-018-3455-3.

[32] Posern K, Linnow K, Niermann M, Kaps C, Steiger M. Thermochemical investigation of the water uptake behavior of MgSO4 hydrates in host materials with different pore size. Thermochim Acta 2015;611:1–9. https://doi.org/10.1016/j.tca.2015.04.031.

[33] Nguyen MH, Zbair M, Dutournié P, Gervasini A, Vaulot C, Bennici S. Toward new low-temperature thermochemical heat storage materials: Investigation of hydration/dehydration behaviors of MgSO4/Hydroxyapatite composite. Sol Energy Mater Sol Cells 2022;240:111696. https://doi.org/10.1016/j.solmat.2022.111696.

[34] Zhang Y, Miao Q, Jia X, Jin Y, Li Z, Tan L, et al. Diatomite-based magnesium sulfate composites for thermochemical energy storage: Preparation and performance investigation. Sol ENERGY 2021;224:907–15. https://doi.org/10.1016/j.solener.2021.05.054.

[35] Miao Q, Zhang Y, Jia X, Tan L, Ding Y. MgSO4-expanded graphite composites for mass and heat transfer enhancement of thermochemical energy storage. Sol Energy 2021;220:432–9. https://doi.org/10.1016/j.solener.2021.03.008.

[36] Mahon D, Claudio G, Eames PC. An experimental investigation to assess the potential of using MgSO 4 impregnation and Mg 2+ ion exchange to enhance the performance of 13X molecular sieves for interseasonal domestic

thermochemical energy storage. Energy Convers Manag 2017;150:870–7. https://doi.org/10.1016/j.enconman.2017.03.080.

[37] Langergen S, Svenska BK. Zur theorie der sogenannten adsoption geloester stoffe. Vetensk Handl 1898;24:1–39.

[38] McKay G. Pseudo-second order model for sorption processes. Proc Biochem 1999;34:451.

[39] Tran HN, You SJ, Hosseini-Bandegharaei A, Chao HP. Mistakes and inconsistencies regarding adsorption of contaminants from aqueous solutions: A critical review. Water Res 2017;120:88–116. https://doi.org/10.1016/j.watres.2017.04.014.

[40] MCLINTOCK IS. The Elovich Equation in Chemisorption Kinetics. Nature 1967;216:1204–5. https://doi.org/10.1038/2161204a0.